Ocean primitive equations and sea level equations

Stephen M. Griffies (NOAA/GFDL and Princeton University)
Based on a lecture given at the school
Advanced School on Earth System Modelling
IITM, Pune, India
July 18-29, 2016
Draft from July 21, 2016

Contents

1 The hydrostatic primitive equations

The ocean is a forced-dissipative dynamical system. Its space-time range of motions extends from the millimetre/second scale of viscous dissipation to the global/centennial scale of climate variations and anthropogenic change. The thermo-hydrodynamical ocean equations are nonlinear, admitting turbulent processes that affect a cascade of mechanical energy and tracer variance across these scales. With increasing integrity of numerical methods and subgrid scale parameterizations, and with enhancements in computer power, ocean general circulation models (OGCMs) have become an essential tool for exploring dynamical interactions within the ocean. OGCMs are also useful to investigate how the ocean interacts with other components of the earth system such as the atmosphere, sea ice, ice shelves, and solid earth. The discrete equations of an OGCM are based on the hydrostatic primitive equations. These equations are formulated by starting from the thermo-hydrodynamical equations for a mass conserving fluid parcel and then assuming the vertical momentum equation reduces to the inviscid hydrostatic balance. We summarize the basics in this section, with far more details available in Griffies (2004), Vallis (2006), and Griffies and Adcroft (2008).

1.1 Mechanical and thermodynamical framework

We formulate the ocean equations by considering a continuum fluid parcel of density ρ, volume δV, mass $\delta M = \rho\,\delta V$, and center of mass velocity

$$\boldsymbol{v} = \boldsymbol{u} + \hat{\boldsymbol{z}}\,w = (u, v, w), \tag{1}$$

with the velocity taken in the frame rotating with the planet. It is most convenient to focus on parcels that conserve mass as they move through the fluid. The linear momentum of the parcel, $\boldsymbol{v}\,\delta M$, evolves according to Newton's Second Law. Forces affecting the large-scale ocean circulation arise from Coriolis (rotating frame), gravity, pressure, and friction, thus leading to the momentum budget

$$\rho\left(\frac{\mathrm{D}}{\mathrm{D}t} + 2\,\boldsymbol{\Omega}\wedge\right)\mathbf{v} = -(\nabla p + \rho\,\nabla\Phi) + \rho\,\boldsymbol{F}. \tag{2}$$

In this equation, $\mathrm{D}/\mathrm{D}t$ is the time derivative taken in the material frame of the moving parcel, $\boldsymbol{\Omega}$ is the rotation vector for the spinning planet, p is the pressure, Φ is the gravitational geopotential, and $\rho\,\boldsymbol{F}$ is the frictional force. The thermo-hydrodynamical equations result from coupling the momentum budget to the First Law of thermodynamics, with the First Law used to determine the evolution of enthalpy, or heat, of the parcel.

The large-scale ocean circulation is generally well approximated by motion of a stably stratified shallow layer of fluid on a rapidly rotating sphere in hydrostatic balance (Vallis, 2006). The hydrostatic ocean primitive equations form the starting point from which OGCM equations are developed, and we write them in the following manner[1]

$$\begin{aligned}
&\text{horizontal momentum} && \rho\left(\frac{\mathrm{D}}{\mathrm{D}t} + \boldsymbol{f}\wedge\right)\boldsymbol{u} = -\nabla_z p + \rho\,\boldsymbol{F} && \text{(3a)}\\
&\text{hydrostatic balance} && \frac{\partial p}{\partial z} = -\rho\,g && \text{(3b)}\\
&\text{mass continuity} && \frac{\mathrm{D}\rho}{\mathrm{D}t} = -\rho\,\nabla\cdot\boldsymbol{v} && \text{(3c)}\\
&\text{tracer conservation} && \rho\left(\frac{\mathrm{D}C}{\mathrm{D}t}\right) = -\nabla\cdot\boldsymbol{J} && \text{(3d)}\\
&\text{equation of state} && \rho = \rho(\Theta, S, p). && \text{(3e)}
\end{aligned}$$

We now detail terms appearing in these equations.

1.2 Linear momentum budget

Equation (3a) provides the budget for horizontal linear momentum. For a hydrostatic fluid, the Coriolis force takes the form $-\rho f\,\hat{\boldsymbol{z}}\wedge\boldsymbol{u}$, with Coriolis parameter

$$\boldsymbol{f} = f\,\hat{\boldsymbol{z}} = (2\,\Omega\,\sin\phi)\,\hat{\boldsymbol{z}}, \tag{4}$$

where $\hat{\boldsymbol{z}}$ is the local vertical direction oriented perpendicular to a surface of constant geopotential, $\Omega \approx 7.29\times10^{-5}\mathrm{s}^{-1}$ is the rotational rate of the earth, and ϕ is the latitude. Linear momentum is also effected by the downgradient horizontal pressure force, $-\nabla_z\,p$. Finally, irreversible exchanges

[1] "Primitive" here refers to the choice to represent the momentum budget in terms of the velocity field rather than the alternative vorticity and divergence.

of momentum between parcels, and between parcels and the ocean boundaries, are parameterized by the friction operator $\rho\,\boldsymbol{F}$. Laplacian and/or biharmonic operators are most commonly used for the friction operator (e.g., Smagorinsky (1993), Griffies and Hallberg (2000), Large et al. (2001), Jochum et al. (2008), Fox-Kemper and Menemenlis (2008)).

Equation (3b) is the vertical momentum equation as approximated by the inviscid hydrostatic balance, with p the hydrostatic pressure and g the gravitational acceleration. The gravitational acceleration is generally assumed constant in space and time for large-scale ocean studies. However, space-time variations of gravity are important when considering tidal motions, as well as changes to the static equilibrium sea level as occur with land ice melt (Section 1.6).

1.3 Mass continuity and the budget for a conservative tracer

The mass continuity equation (3c) arises from constancy of mass for the fluid parcel, $\mathrm{D}\,(\delta M)/\mathrm{D}t = 0$, as well as the kinematic result that the infinitesimal parcel volume is materially modified according to the velocity divergence

$$\frac{1}{\delta V}\frac{\mathrm{D}\,(\delta V)}{\mathrm{D}t} = \nabla \cdot \boldsymbol{v}. \tag{5}$$

The concentration of a material tracer, C, represents the mass of trace constituent per mass of the seawater parcel

$$C = \left(\frac{\text{mass of tracer in parcel}}{\text{mass of seawater in parcel}}\right). \tag{6}$$

Notably, the evolution equation for potential enthalpy (or Conservative Temperature, Θ) takes the same mathematical form as the tracer equation for a conservative material tracer such as salt (McDougall, 2003). Consequently, we can consider Conservative Temperature as the "concentration" of heat.

Although the parcel mass is materially constant, the parcel tracer content and heat are generally modified by subgrid scale mixing or stirring in the presence of concentration gradients. The convergence of the tracer flux vector $\boldsymbol{J}$ incorporates such mixing and stirring processes in the tracer equation (3d). Common means to parameterize these subgrid processes involve diffusive mixing across density surfaces in the ocean interior (diapycnal diffusion as reviewed in MacKinnon et al. (2013)); mixing across geopotential surfaces in the well mixed surface boundary layer (e.g., Large et al. (1994)); diffusive mixing along neutral tangent planes in the interior (Solomon (1971), Redi (1982)); and eddy-induced advection in the ocean interior (e.g., Gent and McWilliams (1990), Gent et al. (1995), Griffies (1998), Fox-Kemper et al. (2013)). Given knowledge of the temperature, salinity, and pressure, we make use of an empirically determined equation of state (equation (3e)) to diagnose the *in situ* density (IOC et al., 2010).

To formulate the discrete equations of an ocean model, we transform the material parcel equations into Eulerian flux-form equations. The flux-form provides a framework for numerical methods that properly conserve mass and linear momentum according to fluxes across grid cell boundaries. In contrast, discretizations based on the material form, also known as the "advective" form, generally lead to spurious sources of scalars and momentum. Spurious scalar sources (e.g., mass, heat, salt, carbon) are particularly unacceptable for climate simulations. Replacing the material time derivative by the Eulerian time derivative and advection

$$\frac{\mathrm{D}}{\mathrm{D}t} = \frac{\partial}{\partial t} + \boldsymbol{v} \cdot \nabla \tag{7}$$

transforms the continuity equation (3c) into

$$\frac{\partial \rho}{\partial t} = -\nabla \cdot (\boldsymbol{v}\,\rho). \tag{8}$$

Likewise, combining the tracer equation (3d) and continuity equation (8) leads to the Eulerian flux-form tracer equation

$$\frac{\partial\,(\rho\,C)}{\partial t} = -\nabla \cdot (\rho\,C\,\boldsymbol{v} + \boldsymbol{J}). \tag{9}$$

Notably, there are no subgrid scale terms on the right hand side of the mass continuity equation (8). This result follows since we formulated the equations for a mass conserving fluid parcel, and made use of the center of mass velocity, $\boldsymbol{v}$ (in Section II.2 of DeGroot and Mazur (1984), they refer to this as the "barycentric" velocity). Operationally, this compatibility between mass and tracer budgets is ensured so long as the subgrid scale flux $\boldsymbol{J}$ vanishes in the presence of a spatially constant tracer concentration, in which case the tracer equation (9) reduces to mass continuity (8).

1.4 Oceanic Boussinesq approximation

The oceanic Boussinesq approximation is based on the observation that dynamically relevant density changes (i.e., changes impacting horizontal pressure gradients) are quite small in the ocean, thus motivating an asymptotic expansion around a global mean density (see Section 9.3 of Griffies and Adcroft (2008)). Operationally, the Boussinesq approximation replaces nearly all occurrances of the *in situ* density in the primitive equations with a constant Boussinesq reference density, ρ_o. The key exception is the hydrostatic balance, where the full density is computed by the equation of state.

When making the Boussinesq approximation, the mass continuity equation (3c) reduces to volume conservation, so that the Boussinesq velocity has zero divergence

$$\nabla \cdot \boldsymbol{v} = 0. \tag{10}$$

Notably, a divergent-free velocity filters out all acoustic modes.

The Boussinesq approximation is based on the scaling $|\boldsymbol{v}^{\mathrm{d}}| \ll |\boldsymbol{v}|$, where $\boldsymbol{v}$ is the prognostic velocity appearing in the Boussinesq momentum equations, and $\boldsymbol{v}^{\mathrm{d}}$ is a divergent velocity field that balances material changes in density through the continuity equation. That is, the divergent velocity field satisfies

$$\frac{\mathrm{D}\rho}{\mathrm{D}t} = -\rho\,\nabla \cdot \boldsymbol{v}^{\mathrm{d}}, \tag{11}$$

where to leading order the material time derivative only involves the non-divergent velocity. It is in this manner that the oceanic Boussinesq approximation admits material density changes from thermohaline effects (i.e., changes in temperature and salinity), which in turn impact the large-scale circulation.

1.5 Virtual salt fluxes versus real water fluxes

A virtual tracer flux ocean model does not transfer water across the ocean boundary. To parameterize impacts from water fluxes on density, salt is transferred across the boundary rather than water (Huang (1993), Griffies et al. (2001), Yin et al. (2010b)). Virtual tracer fluxes are typically associated with rigid lid models, whose volume never changes. Additionally, some free surface ocean climate models also use virtual tracer fluxes (e.g., see Table 1 in Griffies et al. (2014)).

In ocean models, the transport of salt is not associated with a change in ocean mass or volume; i.e., the salt flux does not contribute to the mass flux, Q_{m}, crossing the ocean boundary. Hence, there is no direct mass signal arising from the use of virtual tracer fluxes. Correspondingly, there is no direct bottom pressure nor sea level signal in response to a meltwater flux. The only signal arises from density changes, which are transmitted through baroclinic waves (Stammer, 2008). This limitation further precludes virtual tracer flux models from being used to study changes in the static equilibrium sea level associated with mass redistributions (Section 1.6).

Another limitation of virtual tracer flux models arises from the potentially different responses of the overturning circulation to meltwater pulses. As shown by Yin et al. (2010b), virtual salt flux models tend to exaggerate their freshening effect relative to the response seen in real water flux models. As changes to the Atlantic overturning are thought to be important for regional sea level changes (Yin et al., 2009; Lorbacher et al., 2010), it is useful to remove unnecessary assumptions, such as virtual tracer fluxes, when considering model responses to climate change associated with meltwater events.

1.6 Dynamics with a generalized geopotential

Inhomogeneities in mass distributions cause the earth's gravity field to be non-spherical. These inhomogeneities generally evolve over geological time scales, in which case they are assumed fixed for ocean circulation modelling. However, there is increasing interest in understanding how the ocean responds to mass redistributions associated with melting land ice, with such changes occurring on climate time scales. In particular, such mass redistributions alter the static equilibrium sea level (Farrell and Clark (1976) and Mitrovica et al. (2001)), which defines the surface of a resting ocean. As land ice melts, changes to the static equilibrium sea level will emerge from among changes in dynamical sea level (see Kopp et al. (2010), Slangen et al. (2012), and Slangen et al. (2014)). We are thus prompted to formulate the dynamical equations in the presence of a general geopotential field. This exercise also proves sufficient for considering astronomical tidal forcing.

1.6.1 Geopotentials equal to depth surfaces

The geopotential traditionally used for ocean climate modelling incorporates the effects from gravitational attraction as well as the centrifugal force (e.g., see chapter 2 of Vallis (2006)). The effective gravitational field is conservative, so that the gravitational acceleration of a fluid parcel can be represented as the gradient of a geopotential,

$$\mathbf{g} = -\nabla \Phi, \tag{12}$$

where $\Phi\,(\rho\,\delta V)$ is the gravitational potential energy of a fluid parcel. Surfaces of constant geopotential define surfaces on which the effective gravitational acceleration is constant. In most ocean circulation studies, the geopotential is

$$\Phi = g\,z, \tag{13}$$

with $g \approx 9.8\,\mathrm{m\,s^{-2}}$ the typical gravitational acceleration used in ocean models. In this case, the local vertical direction, $\hat{\boldsymbol{z}}$, is parallel to the effective gravitational acceleration, $\hat{\boldsymbol{z}} \wedge \boldsymbol{g} = 0$. That is, surfaces of constant vertical position, z, are geopotential surfaces.

1.6.2 Geopotentials distinct from depth surfaces

For more general gravitational fields, we write the geopotential as

$$\Phi = g\,(z - \mathcal{H}), \tag{14}$$

where $\mathcal{H} = \mathcal{H}(x, y, z, t)$ incorporates perturbations to the standard geopotential arising from movement of mass and/or astronomical tidal forces.[2] In the presence of this general geopotential, constant depth surfaces, measured by the vertical coordinate z, are no longer equivalent to constant geopotential surfaces. That is, the vertical direction, $\hat{\boldsymbol{z}}$, is not parallel to the effective gravitational acceleration,

$$\boldsymbol{g} = -\nabla\Phi = -g\,(\hat{\boldsymbol{z}} - \nabla\mathcal{H})\,, \tag{15}$$

so that

$$\hat{\boldsymbol{z}} \wedge \boldsymbol{g} = \hat{\boldsymbol{z}} \wedge g\,\nabla\mathcal{H} \neq 0. \tag{16}$$

For applications where gradients in $\mathcal{H}$ dominate the gravity field, it may prove useful to transform the dynamical equations into a geopotential coordinate frame, so that the new vertical direction is parallel to gravity. However, for our purposes, we retain the usual depth coordinate and examine the modifications arising from the generalized geopotential. This approach follows that used for global tide models (e.g., Arbic et al. (2004)).

Making use of the geopotential (14) within the linear momentum equation (2), and then assuming hydrostatic balance holds for the vertical direction, leads to

$$\rho\left(\frac{\mathrm{D}}{\mathrm{D}t} + \hat{\mathbf{z}}\,f\wedge\right)\mathbf{u} = -(\nabla_z\,p + \rho\,\nabla_z\,\Phi) + \rho\,\mathbf{F} \tag{17a}$$

$$\frac{\partial p}{\partial z} = -\rho\,g\left(1 - \frac{\partial\mathcal{H}}{\partial z}\right). \tag{17b}$$

Note that we continue to orient the Coriolis force according to the local vertical direction, $\hat{\boldsymbol{z}}$. However, the pressure gradient is now aligned according to constant geopotential surfaces

$$\nabla_\Phi p = \nabla_z\,p + \rho\,\nabla_z\,\Phi, \tag{18}$$

where $\nabla_z\Phi = -g\,\nabla_z\mathcal{H}$. Buoyancy appearing in the hydrostatic balance is modified by depth dependence of $\mathcal{H}$. Its appearance suggests we introduce a modified gravitational acceleration,

$$g' = g\left(1 - \frac{\partial\mathcal{H}}{\partial z}\right). \tag{19}$$

Alternatively, we may retain a constant gravitational acceleration and introduce the modified density

$$\rho^{(\Phi)} = \rho\left(1 - \frac{\partial\mathcal{H}}{\partial z}\right), \tag{20}$$

in which case the hydrostatic balance becomes

$$\frac{\partial p}{\partial z} = -\rho^{(\Phi)}\,g. \tag{21}$$

No OGCM has incorporated a depth dependent perturbation geopotential field. Indeed, it remains a research question to both formulate the model equations for an ocean with this generalized geopotential, and to examine its role in modifying circulation in the presence of land ice melt. Hence, for simplicity, in the remainder of this chapter we assume

$$\frac{\partial\mathcal{H}}{\partial z} = 0. \tag{22}$$

[2] For astronomical tides, $\mathcal{H} = \mathcal{H}(x, y, t)$ is depth independent (e.g., Section 9.8 in Gill, 1982).

The case of $\mathcal{H} = \mathcal{H}(x, y, t)$ is mathematically identical to the astronomical tide forcing problem. Nonetheless, there has been no consideration of how ocean circulation is impacted by an online interactive calculation of $\mathcal{H}$ under land ice melt scenarios. Only uncoupled studies have been considered, such as those from Kopp et al. (2010) and Slangen et al. (2012). When coupling circulation and gravity models, we expect geopotential changes to propagate via external gravity waves (Section 1.8.2). Consequently, sea level will adjust within a few days towards the new static equilibrium at $z = \mathcal{H}$. If the external mode is cleanly split from internal modes, then we expect no large-scale circulation response to the changing geopotential. However, if there are nontrivial changes to the static equilibrium sea level, particularly near high latitude deep water formation, there may be noticeable impacts on the baroclinic circulation. In that case, a coupled circulation and gravity calculation is required.

1.7 Generalized vertical coordinates

As discussed in Griffies et al. (2000), Griffies et al. (2010), Griffies and Treguier (2013), there are many considerations when choosing vertical the coordinate. Generalized vertical coordinates have thus become a powerful tool for ocean models given their flexibility towards varying applications. They have furthermore become increasingly sophisticated largely due to advances in the Arbitrary Lagrangian-Eulerian (ALE) method. ALE was pioneered in the ocean modelling community by Bleck (2002) (see also discussions by Bleck (2005), Adcroft and Hallberg (2006) and Griffies and Adcroft (2008)).

We write a generalized vertical coordinates as

$$s = s(x, y, z, t), \tag{23}$$

where constant s surfaces monotonically partition the vertical. Transformations from the depth-based primitive equations to generalized vertical coordinates are detailed in Chapter 6 of Griffies (2004). We illustrate the technology by considering the geopotential-aligned pressure gradient (18), which transforms according to

$$\begin{aligned}
\nabla_\Phi p &= \nabla_z p + \rho \nabla_z \Phi && \text{(24a)}\\
&= \left(\nabla_s - \nabla_s z \frac{\partial}{\partial z}\right) p + \rho \left(\nabla_s - \nabla_s z \frac{\partial}{\partial z}\right) \Phi && \text{(24b)}\\
&= \nabla_s p + \rho \nabla_s \Phi, && \text{(24c)}
\end{aligned}$$

where we made use of the hydrostatic balance

$$\frac{\partial p}{\partial z} = -\rho \frac{\partial \Phi}{\partial z}. \tag{25}$$

The expression (24c) means the horizontal momentum equation (17a) remains form invariant under changes to the vertical coordinate.

1.8 Fast and slow dynamics

When developing an economical time steppling algorithm for the primitive equations, it is essential to decompose the dynamics into fast and slow components. Ideally, a decomposition will allow us to time step the fast modes using small time steps, required for numerical stability according to the

CFL constraint (e.g., Durran, 1999), while the slow modes can utilize longer time steps. In general, the CFL constraint means that for any signal of speed U, the time step Δt used in an explicit time stepping scheme must be short enough so that

$$\frac{U\,\Delta t}{\Delta x} \leq 1, \tag{26}$$

where Δx is the grid spacing in either of the horizontal or vertical directions. Hence, our time steps become smaller when the grid spacing is refined (Δx reduces) or when the signal speed increases.

Fast and slow modes generally couple in the ocean, so any attempts to split between the modes is incomplete. This coupling necessitates requires careful treatment by the numerical schemes (see, for example, Killworth et al. (1991), Griffies et al. (2001), chapter 12 of Griffies (2004), Shchepetkin and McWilliams (2005), Hallberg and Adcroft (2009)). Our goal here is to outline steps required to split the dynamics and to then develop a time stepping algorithm. Assumptions built into the algorithms have a direct impact on how sea level dynamics is represented.

1.8.1 Acoustic modes and gravity modes

Acoustic modes are irrelevant for the general circulation. Given that they are faster than gravity waves, it is important to filter acoustic modes from an OGCM so to not be constrained by the CFL condition to take very small time steps. Critically, the vertically propagating acoustic models are filtered by the hydrostatic approximation. Yet a depth independent Lamb wave remains unfiltered, and appears in the non-Boussinesq hydrostatic equations.[3] However, the Lamb mode does not offer any extra constraint on the time stepping beyond that from barotropic gravity waves (see DeSzoeke and Samelson (2002)).

The next modes to consider are the gravity waves, both internal (also called baroclinic) and external (also called barotropic). An external gravity wave rapidly carries information about mass perturbations, which in turn affect the sea level (see Section 1.8.2). In contrast, internal gravity waves carry information about changes in density interfaces within the ocean interior. External gravity waves travel at speeds $(g\,H)^{1/2}$ (H is the ocean depth), which in the deep ocean can be roughly 100 times faster than internal waves (e.g., 100 m s^{-1} versus 1 m s^{-1}). To split between the external and internal motions, we may attempt a formal eigenmode decomposition (e.g., chapter 6 of Gill (1982)). However, that approach works only when the flow is close to linear, which is not always the case in the real ocean. Furthermore, with topography, linear modes are strongly coupled, meaning that a modal decomposition is not theoretically available (Hallberg and Rhines, 1996).

1.8.2 Depth integrated kinematics and dynamics

A practical means to split between external and internal modes is to depth integrate the primitive equations. The depth averaged motions largely capture the external motions, and depth-dependent deviations approximate internal motions. The art associated with these “split-explicit” methods concerns details of the time stepping algorithm, particularly for the fast depth integrated motions, as well as determining what portion of the dynamics to place in the fast versus slow equations.

[3] All acoustic modes are filtered from the Boussinesq fluid due to the non-divergent condition satisified by the velocity field.

We expose some of the issues by formulating the depth integrated kinematics, which is based on a budget for the mass per horizontal area in a column of seawater

$$\frac{\partial}{\partial t}\left(\int_{-H}^{\eta}\rho\,\mathrm{d}z\right) = -\nabla\cdot\boldsymbol{U}^{\rho} + Q_{\mathrm{m}}. \tag{27}$$

That is, the column mass per horizontal area changes according to the convergence of mass transported horizontally by the currents

$$\boldsymbol{U}^{\rho} = \int_{-H}^{\eta}\rho\,\boldsymbol{u}\,\mathrm{d}z, \tag{28}$$

and from mass crossing the ocean free surface, Q_{m}, through precipitation, evaporation, sea ice melt/form, and river runoff. Combining this mass budget (a kinematical balance) to the hydrostatic balance (a dynamical balance) renders a prognostic equation for the difference between the bottom pressure and pressure applied to the ocean surface[4]

$$\frac{1}{g}\frac{\partial\,(p_{\mathrm{b}} - p_{\mathrm{a}})}{\partial t} = -\nabla\cdot\boldsymbol{U}^{\rho} + Q_{\mathrm{m}}. \tag{29}$$

Now consider the horizontal momentum equation for a grid cell, as realized by performing a depth integral over a grid cell of thickness dz (see section 12.2 of Griffies (2004) for relevant manipulations):

$$\left(\frac{\partial}{\partial t} + f\,\hat{\boldsymbol{z}}\wedge\right)(\boldsymbol{u}\,\rho\,\mathrm{d}z) = -\mathrm{d}z\,\nabla_{\Phi}p + \boldsymbol{G}, \tag{30}$$

where $\boldsymbol{G}$ contains advection and friction. To facilitate integrating over the ocean column, we write the pressure gradient in the form

$$\nabla_{\Phi}p = \nabla_{s}p + \rho\,\nabla_{s}\Phi \;=\; \underbrace{\rho\,\nabla_{s}\,\Phi' - (\rho'/\rho_{o})\,\nabla_{s}\,p}_{\text{slow}} \;+\; \underbrace{(\rho/\rho_{o})\,\nabla\,(p_{\mathrm{b}} + \rho_{o}\,\Phi_{\mathrm{b}})}_{\text{fast}}, \tag{31}$$

where p_{b} is the bottom pressure, $\Phi_{\mathrm{b}} = -g\,(H + \mathcal{H})$ is the bottom geopotential, and

$$\Phi'(z) = -g\int_{-H}^{z}\left(\frac{\rho - \rho_{o}}{\rho_{o}}\right)\mathrm{d}z \tag{32}$$

is a geopotential anomaly. The identity (31) can be readily derived by vertically integrating the hydrostatic balance (21) from the ocean bottom to an arbitrary depth. We have labelled terms in this pressure gradient as "slow" and "fast", anticipating how they effect the dynamics.

Now insert the pressure gradient (31) into the momentum budget (30), and then sum over the depth of the ocean to render

$$\left(\frac{\partial}{\partial t} + f\,\hat{\boldsymbol{z}}\wedge\right)\boldsymbol{U}^{\rho} = -\left(\frac{p_{\mathrm{b}} - p_{\mathrm{a}}}{\rho_{o}\,g}\right)\nabla\,(p_{\mathrm{b}} + \rho_{o}\,\Phi_{\mathrm{b}}) + \boldsymbol{H}, \tag{33}$$

where p_{a} is the pressure applied on the top of the ocean from the atmosphere, sea ice, or ice shelf,

$$\boldsymbol{U}^{\rho} = \sum \boldsymbol{u}\,\rho\,\mathrm{d}z \tag{34}$$

[4] We later discuss the bottom and applied surface pressures in Section 2.2.

is the discrete form of the depth integrated horizontal mass transport (see equation (28) for the continuous form), and we made use of the discrete hydrostatic balance

$$g \sum \rho \, \mathrm{d}z = p_{\mathrm{b}} - p_{\mathrm{a}}. \tag{35}$$

The term $\boldsymbol{H}$ contains the vertical sum of $\boldsymbol{G}$ plus the depth integrated slow portion of the pressure gradient.

1.8.3 Linear external gravity waves

To help understand the free linear modes of the depth integrated system, we consider a linearized version of the depth integrated momentum and mass equations. Additionally, ignore drop nonlinear terms, the Coriolis force, and frictional forces, and assume the standard form of the geopotential $\Phi = g\,z$. The result is the linear shallow water system

$$\frac{\partial \boldsymbol{U}^{\rho}}{\partial t} = -H\,\nabla p_{\mathrm{b}} \tag{36a}$$

$$\frac{\partial p_{\mathrm{b}}}{\partial t} = -g\,\nabla \cdot \boldsymbol{U}^{\rho}, \tag{36b}$$

Taking the time derivative of the transport equation (36a) and substituting into the time derivative of the bottom pressure equation (36b) leads to

$$\frac{\partial^2 p_{\mathrm{b}}}{\partial t^2} = g\,H\,\nabla^2 p_{\mathrm{b}}. \tag{37}$$

Likewise, we have

$$\frac{\partial^2 \boldsymbol{U}^{\rho}}{\partial t^2} = g\,H\,\nabla\,(\nabla \cdot \boldsymbol{U}^{\rho}). \tag{38}$$

Each of these equations admits linear wave solutions where the wave signal propagates with speed

$$C_{\mathrm{gravity}} = (g\,H)^{1/2}. \tag{39}$$

These waves transmit information about changes in the bottom pressure, or equivalently changes in the mass per area of a fluid column. Furthermore, assuming the ocean has a constant density, bottom pressure takes the form $p_{\mathrm{b}} = \rho_o\,(H + \eta)$, so that waves in the bottom pressure arise from fluctuations in the sea surface.

1.8.4 Split-explicit algorithm

The essential features of a split-explicit algorithm involve time stepping the depth integrated mass budget (29) and momentum budget (33), making use of small time steps to stably resolve extrernal gravity waves. The slower dynamics is approximated by the full velocity field with the depth averaged velocity removed. The resulting depth dependent motions are dominated by internal gravity waves and advection. The slow dynamics can be integrated with a longer time step than the external motions, which is important since the slow dynamics is three-dimensional and so more expensive computationally. There are many details required to bring these ideas into a working algorithm. The interested reader can find further discussion in chapter 12 of Griffies (2004) and Section 11 of Griffies and Adcroft (2008), along with even more detailed and specialized discussions in Killworth et al. (1991), Griffies et al. (2001), Shchepetkin and McWilliams (2005), and Hallberg and Adcroft (2009).

2 Flavours of sea level tendencies

The upper ocean is typically characterized by breaking surface gravity waves (e.g., Cavaleri et al., 2012), in which case there is no mathematically smooth ocean "surface". Nonetheless, for large-scale hydrostatic modeling, and for large-scale observational oceanography, we define the upper ocean interface as a smooth, non-overturning, permeable, free surface

$$z = \eta(x, y, t) \qquad \text{ocean free surface.} \tag{40}$$

The ocean free surface provides our mathematical representation of sea level. Furthermore, the effects of turbulent wave breaking, which are inherently non-hydrostatic, are incorporated into parameterizations of air-sea boundary fluxes and upper ocean wave induced mixing.

In this section, we explore how sea level changes in time. We already discussed this evolution when considering the fast and slow modes in Section 1.8. Here, we first derive kinematic expressions based on the mass continuity equation. We then make the hydrostatic approximation, which connects changes in sea level to changes in pressure at the ocean top and bottom boundaries. Notably, we here ignore changes in the land-sea boundaries (i.e., the ocean bottom at $z = -H(x, y)$ is static). We also assume the geopotential takes the standard form, $\Phi = g\,z$. We do not consider generalizations based on incorporating a modified gravity field introduced in Section 1.6. Material in this section borrows much from Griffies and Greatbatch (2012) and Griffies et al. (2014).

2.1 Sea level tendencies and mass continuity

We derive a kinematic expression of sea level evolution by integrating the mass continuity equation (3c) over the full ocean depth, and making use of surface and bottom kinematic boundary conditions. The resulting sea level tendency is given by

$$\frac{\partial \eta}{\partial t} = \frac{Q_{\mathrm{m}}}{\rho(\eta)} - \nabla \cdot \mathbf{U} - \int_{-H}^{\eta} \frac{1}{\rho} \frac{\mathrm{D}\rho}{\mathrm{D}t} \, \mathrm{d}z, \tag{41}$$

with

$$\mathbf{U} = \int_{-H}^{\eta} \mathbf{u} \, \mathrm{d}z \tag{42}$$

the vertically integrated horizontal velocity. Equation (41) partitions sea level evolution into a boundary mass flux, Q_{m}, which is the mass per time per horizontal area of precipitation - evaporation + runoff that crosses the ocean surface; the convergence of vertically integrated horizontal ocean currents; and material changes in density.

The sea level equation (41) reveals that the direct impact on sea level from ocean currents is to redistribute ocean volume through the convergence term, $-\nabla \cdot \mathbf{U}$. However, this term does not alter the global mean sea level, since its global integral vanishes. This equation thus offers a very useful analysis framework to study how physical processes impact on global mean sea level. Namely, the explicit appearance of ocean currents is eliminated when forming the global integral of equation (41), leaving only surface boundary fluxes and material density changes (Griffies and Greatbatch, 2012).

The *non-Boussinesq steric effect* refers to sea level changes associated with material density changes

$$\left(\frac{\partial \eta}{\partial t}\right)^{\text{non-Bouss steric}} = -\int_{-H}^{\eta} \frac{1}{\rho} \frac{\mathrm{D}\rho}{\mathrm{D}t} \, \mathrm{d}z. \tag{43}$$

This term is absent in Boussinesq fluids (Section 1.4). That is, Boussinesq kinematics is based on conserving volume, not mass, and integrating over a seawater column leads to the Boussinesq sea level equation

$$\left(\frac{\partial \eta}{\partial t}\right)^{\text{bouss}} = \frac{Q_{\text{m}}}{\rho_o} - \nabla \cdot \mathbf{U}. \tag{44}$$

As discussed by Losch et al. (2004) and Griffies and Greatbatch (2012), Boussinesq and non-Boussinesq fluids capture very similar large-scale patterns of dynamical sea level.[5] However, Boussinesq fluids require an adjustment of their prognosed sea level to capture the global mean of the non-Boussinesq fluid. For example, Greatbatch (1994) noted that a Boussinesq fluid will not alter its prognostic sea level under a uniform heating. Global mean sea level changes from heating are captured when retaining the mass conserving kinematics of a non-Boussinesq fluid. Fortunately, a time dependent global adjustment to the Boussinesq sea level is generally sufficient to recover the non-Boussinesq results (Greatbatch (1994), Griffies and Greatbatch (2012)).

2.2 Sea level tendencies and the hydrostatic balance

We now deduce relations for sea level evolution based on the hydrostatic balance (3b). Vertically integrating this balance from the ocean bottom at $z = -H(x, y)$ to the surface at $z = \eta(x, y, t)$, leads to the expression

$$p_{\text{b}} = p_{\text{a}} + g \int_{-H}^{\eta} \rho \, \mathrm{d}z. \tag{45}$$

The bottom pressure, p_{b}, equals to the sum of the pressure applied at the sea surface, p_{a} (e.g., from the atmosphere, sea ice, and ice shelf), plus the weight per horizontal area of seawater in the liquid ocean column. This balance holds instantaneously. Consequently, for example, adding mass to the ocean surface instantaneously increases bottom pressure, no matter how deep the ocean. Such instantaneous signal propagation results from assuming a hydrostatic balance, in which acoustic modes are removed (in effect, they have infinite speed). For a non-hydrostatic fluid, vertically propagating acoustic waves propagate the pressure signal at a finite speed.

Taking the time derivative of the bottom pressure equation (45) renders

$$\frac{\partial\,(p_{\text{b}} - p_{\text{a}})}{\partial t} = g\,\rho(\eta)\,\frac{\partial \eta}{\partial t} + g \int_{-H}^{\eta} \frac{\partial \rho}{\partial t}\,\mathrm{d}z. \tag{46}$$

where $\rho(\eta) = \rho(z = \eta)$ is density at the ocean free surface. This equation represents a diagnostic balance between three tendencies, whereby changes in the mass of seawater in an ocean column (left hand side) are balanced by changes in the sea level and depth integrated changes in density (local steric effects). Following Gill and Niiler (1973), we rearrange to yield a diagnostic expression for the sea level tendency

$$\frac{\partial \eta}{\partial t} = \underbrace{\left(\frac{1}{g\,\rho(\eta)}\right)\frac{\partial\,(p_{\text{b}} - p_{\text{a}})}{\partial t}}_{\text{mass tendency}} - \underbrace{\frac{1}{\rho(\eta)} \int_{-H}^{\eta} \frac{\partial \rho}{\partial t}\,\mathrm{d}z}_{\text{local steric tendency}}. \tag{47}$$

This decomposition connects changes in ocean volume to changes in ocean mass and changes in ocean density. It provides the basis for various diagnostic analyses of regional sea level changes

[5] Dynamic sea level refers to the sea level normalized to have zero area mean. This component of sea level responds directly to dynamical processes in the ocean.

in models and observations, with examples given by Lowe and Gregory (2006), Landerer et al. (2007b), Landerer et al. (2007a), Yin et al. (2009), Yin et al. (2010a), Pardaens et al. (2011), Griffies et al. (2014), and Landerer et al. (2015). One key reason this decomposition is so useful is that each term, in principle, can be independently measured using methods of observational oceanography, and tested by comparing to global model simulations. Namely, the sea level tendency is measured by satellite altimetry (e.g., this book); the mass tendency is measured by the gravity field (e.g., GRACE); and the density (or *local steric*) term is measured by *in situ* temperature and salinity (e.g., Argo). We discuss facets of this balance in the following.

2.2.1 Sea level tendencies due to mass changes

The hydrostatic balance (45) indicates that the pressure difference $p_b - p_a$ changes when mass per area within a seawater column changes. Furthermore, the column mass budget is given by equation (27), which allows us to write the equivalent expressions for sea level change arising from mass changes

$$\left(\frac{\partial \eta}{\partial t}\right)^{\text{mass changes}} = \underbrace{\left(\frac{1}{g\,\rho(\eta)}\right)\frac{\partial\,(p_b - p_a)}{\partial t}}_{\text{mass tendency}} = \underbrace{\frac{-\nabla \cdot \boldsymbol{U}^{\rho} + Q_m}{\rho(\eta)}}_{\text{mass convergence}}. \tag{48}$$

Mass converging to a column causes the column to increase its thickness and thus to raise the sea level. Signals of mass changes propagate through barotropic wave processes (Section 1.8.2), which rapidly transmit mass induced sea level changes around the World Ocean (e.g., see Lorbacher et al. (2012)).

2.2.2 Sea level tendencies due to local steric changes

The second term on the right hand side of equation (47) arises from local depth integrated density changes, which we refer to as the *local steric* effect

$$\left(\frac{\partial \eta}{\partial t}\right)^{\text{local steric}} = -\frac{1}{\rho(\eta)} \int_{-H}^{\eta} \frac{\partial \rho}{\partial t}\,\mathrm{d}z. \tag{49}$$

This local steric effect is distinguished from the non-Boussinesq steric effect discussed in Section 2.1.

As density in the column decreases, such as when a fluid column warms or freshens, then the column expands and sea level rises. The local steric term in equation (49) thus arises from changes in temperature, salinity (and pressure).[6] In many regions, such as the Atlantic, the ocean is both warming and getting saltier, so that the *thermosteric* (temperature induced) sea level rise is partially compensated by *halosteric* (salinity induced) sea level fall. We illustrate this point in Figure **??**, taken from a climate model simulation of climate change. Finally, we note that changes in steric sea level propagate throughout the World Ocean on a baroclinic time scale, so are far slower than the barotropic signals that transmit mass changes (Bryan (1996), Hsieh and Bryan (1996), Stammer (2008), and Lorbacher et al. (2012)).

[6]Pressure-induced changes are generally subdominant, so that the local steric effect is predominantly determined by changes in temperature and salinity.

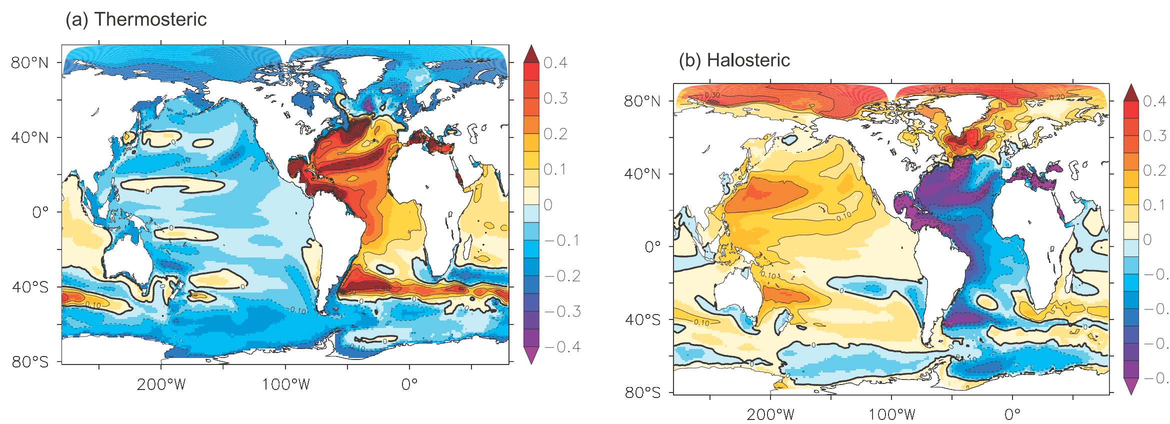

Figure 1: Thermosteric and halosteric contributions to sea level changes as realised in a climate change simulation using the GFDL-CM2.1 coupled climate model. Shown are differences from the control simulations averaged over years 2091-2100, relative to a control simulation at year 1981-2000. These figures are taken from Yin et al. (2010a).

2.2.3 Inverse barometer sea level tendencies

Consider changes to the pressure applied to the sea surface, yet keep the ocean bottom pressure and ocean density unchanged. We can realize this situation so long as the sea level adjusts to provide exact compensation for changes in the applied pressure. Making use of equation (47) renders

$$\left(\frac{\partial \eta}{\partial t}\right)^{\text{inverse barometer}} = -\left(\frac{1}{g\,\rho(\eta)}\right)\frac{\partial p_{\mathrm{a}}}{\partial t}. \tag{50}$$

As reviewed in Appendix C of Griffies and Greatbatch (2012), such *inverse barometer* responses of sea level are commonly realized under sea ice and under atmospheric pressure loading. Although sea level changes, the "effective sea level"

$$\eta' = \eta + \left(\frac{p_{\mathrm{a}}}{g\,\overline{\rho}}\right) \tag{51}$$

remains close to constant, where we introduced the area mean surface density, $\overline{\rho}$. For example, the sea level is depressed if the applied pressure increases. If the depressed sea level maintains an inverse barometer response, then the effective sea level remains unchanged.

2.2.4 Sea level tendencies, dynamic topography, and the rigid lid

Following Appendix B.4 of Griffies et al. (2014), consider the thickness of fluid extending from the ocean surface to a chosen pressure level in the ocean interior, as given by

$$\mathcal{D}(\mathcal{P}) = \eta - z(\mathcal{P}). \tag{52}$$

We may relate this expression to the integral of the specific volume, ρ^{-1}, between two pressure surfaces

$$\mathcal{D}(\mathcal{P}) = \int_{z(\mathcal{P})}^{\eta} \mathrm{d}z = \int_{p_{\mathrm{a}}}^{\mathcal{P}} \frac{\mathrm{d}p}{g\,\rho}, \tag{53}$$

where the second step used the hydrostatic balance to relate changes in pressure to changes in thickness, $\mathrm{d}p = -g\,\rho\,\mathrm{d}z$. We refer to the thickness $\mathcal{D}(\mathcal{P})$ as the *dynamic topography* with respect to a reference pressure $\mathcal{P}$. Evolution of the dynamic topography arises from changes in the applied pressure, and changes in the specific volume

$$g\,\frac{\partial\,\mathcal{D}(\mathcal{P})}{\partial t} = -\frac{1}{\rho(\eta)}\frac{\partial p_{\mathrm{a}}}{\partial t} + \int\limits_{p_{\mathrm{a}}}^{\mathcal{P}} \frac{\partial \rho^{-1}}{\partial t}\,\mathrm{d}p, \tag{54}$$

where the time derivative acting on the specific volume is taken on surfaces of constant pressure.

By the definition (52), if the depth $z(\mathcal{P})$ of the constant pressure surface is static, then the layer thickness $\mathcal{D}(\mathcal{P})$ evolution matches that of the sea level η. However, there is generally no such static pressure level, thus making the time tendencies differ. Nonetheless, for lack of sufficient information about deep ocean currents, it is sometimes convenient in dynamical oceanography to assume a pressure at which baroclinic currents vanish (e.g., Pond and Pickard (1983), Tomczak and Godfrey (1994)). This *level of no motion* occurs if the barotropic pressure head associated with a sea level undulation is exactly compensated by density structure within the ocean interior (see Figure 2). Currents are static below the level of no motion and so are dynamically disconnected from sea level changes. Evolution of the column thickness between the surface and the level of no motion thus provides a proxy for the evolution of sea level.

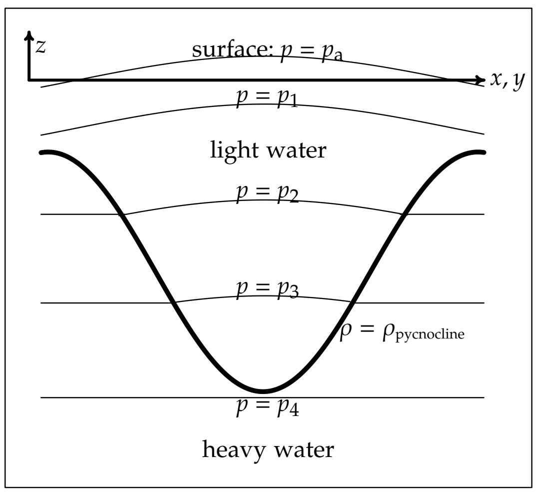

Figure 2: A vertical slice through a 1.5 layer ocean in hydrostatic balance, taken after Figure 3.3 from Tomczak and Godfrey (1994). Shown here is a plug of light water, as may occur in a warm core eddy, sitting on top of heavy water, where motion is assumed to vanish in the heavy water. The sea surface experiences an applied pressure $p = p_{\mathrm{a}}$, assumed to be uniform for this idealized situation. Isolines of hydrostatic pressure are shown, with a slight upward bow to the isobars within the light water region, and flat isobars beneath, in the region of zero motion. Note how sea level is a maximum above the pycnocline minimum, which occurs due to baroclinic compensation. The slope of the pycnocline is about 100-300 times larger than the sea level (Rule 1a of Tomczak and Godfrey, 1994). See Appendix B of Griffies et al. (2014) for more details.

Analyses based on assuming a level of no motion are common in simulations with a rigid lid ocean model, as in the studies of Delworth et al. (1993), Bryan (1996), Griffies and Bryan

(1997). As there is no tendency equation for the free surface in rigid lid models, only indirect methods are available for obtaining information about sea level time changes (Gregory et al., 2001). Furthermore, given the records of observed hydrography, one may find it convenient to consider dynamic topography as a proxy for dynamic sea level (e.g., Levitus, 1990).

3 Sea level gradients and ocean circulation

From the hydrostatic balance (3b), we can write the pressure at an arbitrary point z in the form

$$p(z) = p_{\rm a} + g \int_z^\eta \rho \, {\rm d}z', \tag{55}$$

which then leads to the horizontal pressure gradient

$$\nabla_z p(z) = \nabla p_{\rm a} + g\,\rho(\eta)\,\nabla\eta + g \int_z^\eta \nabla_z \rho \, {\rm d}z' \tag{56a}$$

$$\approx g\,\overline{\rho}\,\nabla\eta' + g \int_z^\eta \nabla_z \rho \, {\rm d}z', \tag{56b}$$

where we introduced the effective sea level (equation (51)) discussed in relation to the inverse barometer.

3.1 Surface ocean

A particularly simple relation between sea level and ocean currents occurs when the surface ocean flow is in geostrophic balance, in which

$$g\,\nabla\eta' = -f\,\hat{\mathbf{z}} \wedge \mathbf{u}, \tag{57}$$

where $\mathbf{u}$ is the surface horizontal velocity. This equation forms the basis for how surface ocean currents are diagnosed from sea level measurements (Wunsch and Stammer, 1998). A slight generalization is found by including the turbulent momentum flux $\boldsymbol{\tau}^{\rm s}$ through the ocean surface boundary, in which case the sea level gradient takes the form

$$g\,\nabla\eta' = -f\,\hat{\mathbf{z}} \wedge \mathbf{u} + \frac{\boldsymbol{\tau}^{\rm s}}{\rho_o\,h_{\rm E}}, \tag{58}$$

where $h_{\rm E}$ is the Ekman depth over which the boundary stresses penetrate the upper ocean. As noted by Lowe and Gregory (2006), surface currents in balance with surface wind stresses tend to flow parallel to the sea level gradient, whereas geostrophically balanced surface currents are aligned with surfaces of constant sea level.

3.2 Full ocean column

Vertically integrating the linearized form of the horizontal momentum budget (3a) in the absence of horizontal friction leads to the relation

$$(g\,\rho_o\,H)\,\nabla\eta' = \boldsymbol{\tau}^{\rm s} + Q_{\rm m}\,\mathbf{u}_{\rm m} - \boldsymbol{\tau}^{\rm b} - (\partial_t + f\,\hat{\mathbf{z}}\wedge)\,\mathbf{U}^{\rho} - \mathbf{B}. \tag{59}$$

In this equation, $\boldsymbol{\tau}^{\mathrm{s}}$ and $\boldsymbol{\tau}^{\mathrm{b}}$ are the turbulent boundary momentum fluxes at the surface and bottom; $Q_{\mathrm{m}}\, \mathbf{u}_{\mathrm{m}}$ is the horizontal advective momentum flux associated with surface boundary fluxes of mass, with $\mathbf{u}_{\mathrm{m}}$ the horizontal momentum per mass of material crossing the ocean surface.[7] Finally,

$$\mathbf{B} = g \int_{-H}^{\eta} \mathrm{d}z \int_{z}^{\eta} \nabla_z \rho \, \mathrm{d}z' \tag{60}$$

is a horizontal pressure gradient arising from horizontal density gradients throughout the ocean column. Lowe and Gregory (2006) employed the steady state version of the balance (59) while ignoring boundary terms (see their equation (7)),

$$(g\, \rho_o\, H)\, \nabla \eta' \approx -f\, \hat{\mathbf{z}} \wedge \mathbf{U}^{\rho} - \mathbf{B} \tag{61}$$

to help interpret the sea level patterns in their climate model simulations.

3.3 Barotropic geostrophic balance

As seen by equation (59), sea level gradients balance many terms, including surface fluxes, internal pressure gradients, and vertically integrated transport. Dropping all terms except Coriolis leads to a geostrophic balance for the vertically integrated flow, whereby equation (59) reduces to

$$(g\, \rho_o\, H)\, \nabla \eta' = f\, \hat{\mathbf{z}} \wedge \mathbf{U}^{\rho}, \tag{62}$$

which is equivalent to

$$\mathbf{U}^{\rho} = -\left(\frac{g\, \rho_o\, H}{f}\right) \hat{\mathbf{z}} \wedge \nabla \eta'. \tag{63}$$

With a constant depth and Coriolis parameter, the effective sea level is the streamfunction for the vertically integrated flow.

Following Wunsch and Stammer (1998), we use equation (62) to see how much vertically integrated transport is associated with a sea level deviation. For example, the meridional transport between two longitudes x_1 and x_2 is given by

$$\int_{x_1}^{x_2} \mathrm{d}x\, V^{\rho} = \frac{g\, \rho_o\, H}{f}\, [\eta(x_2) - \eta(x_1)], \tag{64}$$

where we assumed a flat ocean bottom. The horizontal distance drops out from the right hand side, so that the meridional geostrophic transport depends only on the sea level difference across the zonal section, and not on the length of the section. Assume the ocean depth is $H = 4000$ m and set $f = 7.3 \times 10^{-5}\ \mathrm{s}^{-1}$ (30° latitude), which renders a transport of about $6 \times 10^{9}\ \mathrm{kg\ s}^{-1}$, or six Sverdrups.

References

Adcroft, A., and R. Hallberg, 2006: On methods for solving the oceanic equations of motion in generalized vertical coordinates. *Ocean Modelling*, **11**, 224–233.

[7] In ocean models, $\mathbf{u}_{\mathrm{m}}$ is generally taken as the surface ocean horizontal velocity.

Arbic, B., S. T. Garner, R. W. Hallberg, and H. L. Simmons, 2004: The accuracy of surface elevations in forward global barotropic and baroclinic tide models. *Deep Sea Research*, **51**, 3069–3101.

Bleck, R., 2002: An oceanic general circulation model framed in hybrid isopycnic-cartesian coordinates. *Ocean Modelling*, **4**, 55–88.

Bleck, R., 2005: On the use of hybrid vertical coordinates in ocean circulation modeling. *Ocean Weather Forecasting: an Integrated View of Oceanography*, E. P. Chassignet, and J. Verron, Eds., Vol. 577, Springer, 109–126.

Bryan, K., 1996: The steric component of sea level rise associated with enhanced greenhouse warming: a model study. *Climate Dynamics*, **12**, 545–555.

Cavaleri, L., B. Fox-Kemper, and M. Hemer, 2012: Wind waves in the coupled climate system. *Bulletin of the American Meteorological Society*, **93**, 1651–1661, doi:10.1175/BAMS-D-11-00170.1.

DeGroot, S. R., and P. Mazur, 1984: *Non-Equilibrium Thermodynamics*. Dover Publications, New York, 510 pp.

Delworth, T. L., S. Manabe, and R. J. Stouffer, 1993: Interdecadal variations of the thermohaline circulation in a coupled ocean-atmosphere model. *Journal of Climate*, **6**, 1993–2011.

DeSzoeke, R. A., and R. M. Samelson, 2002: The duality between the Boussinesq and non-Boussinesq hydrostatic equations of motion. *Journal of Physical Oceanography*, **32**, 2194–2203.

Durran, D. R., 1999: *Numerical Methods for Wave Equations in Geophysical Fluid Dynamics*. Springer Verlag, Berlin, 470 pp.

Farrell, W., and J. Clark, 1976: On postglacial sea level. *Geophysical Journal of the Royal Astronomical Society*, **46**, 646–667.

Fox-Kemper, B., R. Lumpkin, and F. Bryan, 2013: Lateral transport in the ocean interior. *Ocean Circulation and Climate, 2nd Edition: A 21st Century Perspective*, G. Siedler, S. M. Griffies, J. Gould, and J. Church, Eds., International Geophysics Series, Vol. 103, Academic Press, 185–209.

Fox-Kemper, B., and D. Menemenlis, 2008: Can large eddy simulation techniques improve mesoscale rich ocean models? *Ocean Modeling in an Eddying Regime*, M. Hecht, and H. Hasumi, Eds., Geophysical Monograph, Vol. 177, American Geophysical Union, 319–338.

Gent, P. R., and J. C. McWilliams, 1990: Isopycnal mixing in ocean circulation models. *Journal of Physical Oceanography*, **20**, 150–155.

Gent, P. R., J. Willebrand, T. J. McDougall, and J. C. McWilliams, 1995: Parameterizing eddy-induced tracer transports in ocean circulation models. *Journal of Physical Oceanography*, **25**, 463–474.

Gill, A., 1982: *Atmosphere-Ocean Dynamics*, International Geophysics Series, Vol. 30. Academic Press, London, 662 + xv pp.

Gill, A. E., and P. Niiler, 1973: The theory of the seasonal variability in the ocean. *Deep-Sea Research*, **20 (9)**, 141–177.

Greatbatch, R. J., 1994: A note on the representation of steric sea level in models that conserve volume rather than mass. *Journal of Geophysical Research*, **99**, 12 767–12 771.

Gregory, J., and Coauthors, 2001: Comparison of results from several AOGCMs for global and regional sea-level change 1900–2100. *Climate Dynamics*, **18**, 225–240.

Griffies, S. M., 1998: The Gent-McWilliams skew-flux. *Journal of Physical Oceanography*, **28**, 831–841.

Griffies, S. M., 2004: *Fundamentals of Ocean Climate Models*. Princeton University Press, Princeton, USA, 518+xxxiv pages.

Griffies, S. M., and A. J. Adcroft, 2008: Formulating the equations for ocean models. *Ocean Modeling in an Eddying Regime*, M. Hecht, and H. Hasumi, Eds., Geophysical Monograph, Vol. 177, American Geophysical Union, 281–317.

Griffies, S. M., and K. Bryan, 1997: A predictability study of simulated North Atlantic multidecadal variability. *Climate Dynamics*, **13**, 459–487.

Griffies, S. M., and R. J. Greatbatch, 2012: Physical processes that impact the evolution of global mean sea level in ocean climate models. *Ocean Modelling*, **51**, 37–72, doi:10.1016/j.ocemod.2012.04.003.

Griffies, S. M., and R. W. Hallberg, 2000: Biharmonic friction with a Smagorinsky viscosity for use in large-scale eddy-permitting ocean models. *Monthly Weather Review*, **128**, 2935–2946.

Griffies, S. M., R. Pacanowski, M. Schmidt, and V. Balaji, 2001: Tracer conservation with an explicit free surface method for z-coordinate ocean models. *Monthly Weather Review*, **129**, 1081–1098.

Griffies, S. M., and A.-M. Treguier, 2013: Ocean models and ocean modeling. *Ocean Circulation and Climate, 2nd Edition: A 21st Century Perspective*, G. Siedler, S. M. Griffies, J. Gould, and J. Church, Eds., International Geophysics Series, Vol. 103, Academic Press, 521–552.

Griffies, S. M., and Coauthors, 2000: Developments in ocean climate modelling. *Ocean Modelling*, **2**, 123–192.

Griffies, S. M., and Coauthors, 2010: Problems and prospects in large-scale ocean circulation models. *Proceedings of the OceanObs09 Conference: Sustained Ocean Observations and Information for Society, Venice, Italy, 21-25 September 2009*, J. Hall, D. Harrison, and D. Stammer, Eds., Vol. 2, ESA Publication WPP-306.

Griffies, S. M., and Coauthors, 2014: An assessment of global and regional sea level for years 1993-2007 in a suite of interannual CORE-II simulations. *Ocean Modelling*, **78**, 35–89, doi:10.1016/j.ocemod.2014.03.004.

Hallberg, R., and A. Adcroft, 2009: Reconciling estimates of the free surface height in lagrangian vertical coordinate ocean models with mode-split time stepping. *Ocean Modelling*, **29**, 15–26.

Hallberg, R., and P. Rhines, 1996: Buoyancy-driven circulation in a ocean basin with isopycnals intersectin the sloping boundary. *Journal of Physical Oceanography*, **26**, 913–940.

Hsieh, W., and K. Bryan, 1996: Redistribution of sea level rise associated with enhanced greenhouse warming: a simple model study. *Climate Dynamics*, **12**, 535–544.

Huang, R. X., 1993: Real freshwater flux as a natural boundary condition for the salinity balance and thermohaline circulation forced by evaporation and precipitation. *Journal of Physical Oceanography*, **23**, 2428–2446.

IOC, SCOR, and IAPSO, 2010: *The international thermodynamic equation of seawater-2010: calculation and use of thermodynamic properties*. Intergovernmental Oceanographic Commission, Manuals and Guides No. 56, UNESCO, available from http://www.TEOS-10.org, 196pp.

Jochum, M., , G. Danabasoglu, M. Holland, Y.-O. Kwon, and W. Large, 2008: Ocean viscosity and climate. *Journal of Geophysical Research*, **114 C06017**, doi:10.1029/2007JC004515.

Killworth, P. D., D. Stainforth, D. J. Webb, and S. M. Paterson, 1991: The development of a free-surface Bryan-Cox-Semtner ocean model. *Journal of Physical Oceanography*, **21**, 1333–1348.

Kopp, R. E., J. X. Mitrovica, S. M. Griffies, J. Yin, C. C. Hay, and R. J. Stouffer, 2010: The impact of Greenland melt on regional sea level: a preliminary comparison of dynamic and static equilibrium effects. *Climatic Change Letters*, **103**, 619–625, doi:10.1007/s10584-010-9935-1.

Landerer, F., J. Jungclaus, and J. Marotzke, 2007a: Ocean bottom pressure changes lead to a decreasing length-of-day in a warming climate. *Geophysical Research Letters*, **34-L06307**, doi: 10.1029/2006GL029106.

Landerer, F., J. Jungclaus, and J. Marotzke, 2007b: Regional dynamic and steric sea level change in response to the IPCC-A1B Scenario. *Journal of Physical Oceanography*, **37**, 296–312.

Landerer, F., D. N. Wiese, K. Bentel, C. Boening, and M. Watkins, 2015: North Atlantic meridional overturning circulation variations from GRACE ocean bottom pressure anomalies. *Geophysical Research Letters*, **42**, 8114–8121, doi:10.1002/2015GL065730.

Large, W., J. McWilliams, and S. Doney, 1994: Oceanic vertical mixing: a review and a model with a nonlocal boundary layer parameterization. *Reviews of Geophysics*, **32**, 363–403.

Large, W. G., G. Danabasoglu, J. C. McWilliams, P. R. Gent, and F. O. Bryan, 2001: Equatorial circulation of a global ocean climate model with anisotropic horizontal viscosity. *Journal of Physical Oceanography*, **31**, 518–536.

Levitus, S., 1990: Multipentadal variability of steric sea level and geopotential thickness of the north atlantic ocean, 1970-1974 versus 1955-1959. *Journal of Geophysical Research*, **95**, 5233–5238.

Lorbacher, K., J. Dengg, C. Böning, and A. Biastoch, 2010: Regional patterns of sea level change related to interannual variability and multidecadal trends in the Atlantic Meridional Overturning Circulation. *Journal of Physical Oceanography*, **23**, 4243–4254.

Lorbacher, K., S. J. Marsland, J. A. Church, S. M. Griffies, and D. Stammer, 2012: Rapid barotropic sea-level rise from ice-sheet melting scenarios. *Journal of Geophysical Research*, **117, C06003**, doi: 10.1029/2011JC007733.

Losch, M., A. Adcroft, and J.-M. Campin, 2004: How sensitive are coarse general circulation models to fundamental approximations in the equations of motion? *Journal of Physical Oceanography*, **34**, 306–319.

Lowe, J. A., and J. M. Gregory, 2006: Understanding projections of sea level rise in a hadley centre coupled climate model. *Journal of Geophysical Research: Oceans*, **111 (C11)**, n/a–n/a, doi: 10.1029/2005JC003421, URL http://dx.doi.org/10.1029/2005JC003421.

MacKinnon, J., Louis St. Laurent, and A. N. Garabato, 2013: Diapycnal mixing processes in the ocean interior. *Ocean Circulation and Climate, 2nd Edition: A 21st century perspective*, G. Siedler, S. M. Griffies, J. Gould, and J. Church, Eds., International Geophysics Series, Vol. 103, Academic Press, 159–183.

McDougall, T. J., 2003: Potential enthalpy: a conservative oceanic variable for evaluating heat content and heat fluxes. *Journal of Physical Oceanography*, **33**, 945–963.

Mitrovica, J. X., M. E. Tamisiea, J. L. Davis, and G. A. Milne, 2001: Recent mass balance of polar ice sheets inferred from patterns of global sea-level change. *Nature*, **409**, 1026–1029.

Pardaens, A., J. Gregory, and J. Lowe, 2011: A model study of factors influencing projected changes in regional sea level over the twenty-first century. *Climate Dynamics*, 10.1029/2011GL047678, doi: DOI10.1007/s00382-009-0738-x.

Pond, S., and G. L. Pickard, 1983: *Introductory Dynamical Oceanography*. 2nd ed., Pergamon Press, Oxford.

Redi, M. H., 1982: Oceanic isopycnal mixing by coordinate rotation. *Journal of Physical Oceanography*, **12**, 1154–1158.

Shchepetkin, A., and J. McWilliams, 2005: The regional oceanic modeling system (ROMS): a split-explicit, free-surface, topography-following-coordinate oceanic model. *Ocean Modelling*, **9**, 347–404.

Slangen, A., C. Katsman, R. van de Wal, L. Vermeersen, and R. Riva, 2012: Towards regional projections of twenty-first century sea-level change based on IPCC SRES scenarios. *Climate Dynamics*, 10.1007/s00 382–011–1057–6.

Slangen, A., son, C. Katsman, R. van de Wal, A. Hoehl, L. Vermeersen, and D. Stammer, 2014: Projecting twenty-first century regional sea-level changes. *Climatic Change*, 317–332.

Smagorinsky, J., 1993: Some historical remarks on the use of nonlinear viscosities. *Large Eddy Simulation of Complex Engineering and Geophysical Flows*, B. Galperin, and S. A. Orszag, Eds., Cambridge University Press, 3–36.

Solomon, H., 1971: On the representation of isentropic mixing in ocean models. *Journal of Physical Oceanography*, **1**, 233–234.

Stammer, D., 2008: Response of the global ocean to Greenland and Antarctic ice melting. *Journal of Geophysical Research*, **113**, doi:10.1029/2006JC004079.

Tomczak, M., and J. S. Godfrey, 1994: *Regional Oceanography: An Introduction*. Pergamon Press, Oxford, England, 422 + vii pp.

Vallis, G. K., 2006: *Atmospheric and Oceanic Fluid Dynamics: Fundamentals and Large-scale Circulation*. 1st ed., Cambridge University Press, Cambridge, 745 + xxv pp.

Wunsch, C., and D. Stammer, 1998: Satellite altimetry, the marine geoid, and the oceanic general circulation. *Annual Reviews of Earth Planetary Science*, **26**, 219–253.

Yin, J., S. M. Griffies, and R. Stouffer, 2010a: Spatial variability of sea-level rise in 21st century projections. *Journal of Climate*, **23**, 4585–4607.

Yin, J., M. Schlesinger, and R. Stouffer, 2009: Model projections of rapid sea-level rise on the northeast coast of the United States. *Nature Geosciences*, **2**, 262–266, doi:10.1038/NGEO462.

Yin, J., R. Stouffer, M. J. Spelman, and S. M. Griffies, 2010b: Evaluating the uncertainty induced by the virtual salt flux assumption in climate simulations and future projections. *Journal of Climate*, **23**, 80–96.